Published April 18, 2016

A requirement for filopodia extension toward Slit during Robo-mediated axon repulsion

Russell E. McConnell,[1] J. Edward van Veen,[1,2] Marina Vidaki,[1] Adam V. Kwiatkowski,[2] Aaron S. Meyer,[1,3] and Frank B. Gertler[1,2]

[1]David H. Koch Institute for Integrative Cancer Research, [2]Department of Biology, and [3]Department of Biological Engineering, Massachusetts Institute of Technology, Cambridge, MA 01239

Axons navigate long distances through complex 3D environments to interconnect the nervous system during development. Although the precise spatiotemporal effects of most axon guidance cues remain poorly characterized, a prevailing model posits that attractive guidance cues stimulate actin polymerization in neuronal growth cones whereas repulsive cues induce actin disassembly. Contrary to this model, we find that the repulsive guidance cue Slit stimulates the formation and elongation of actin-based filopodia from mouse dorsal root ganglion growth cones. Surprisingly, filopodia form and elongate toward sources of Slit, a response that we find is required for subsequent axonal repulsion away from Slit. Mechanistically, Slit evokes changes in filopodium dynamics by increasing direct binding of its receptor, Robo, to members of the actin-regulatory Ena/VASP family. Perturbing filopodium dynamics pharmacologically or genetically disrupts Slit-mediated repulsion and produces severe axon guidance defects in vivo. Thus, Slit locally stimulates directional filopodial extension, a process that is required for subsequent axonal repulsion downstream of the Robo receptor.

Introduction

Growth cones are motile structures at the distal ends of axons that translate extracellular signals into directional responses, enabling axons to navigate to their proper targets (Lowery and Van Vactor, 2009). Morphologically, growth cones are characterized by two types of F-actin–supported structures: lamellipodia and filopodia. Lamellipodia are sheet-like protrusions supported by a branched actin network formed by the Arp2/3 complex, whereas filopodia are rod-like protrusions supported by unbranched parallel bundles of actin filaments formed by Ena/VASP and formin family proteins (Dent et al., 2011; Gomez and Letourneau, 2014). Ena/VASP proteins increase actin polymerization rates and promote the elongation of long, unbranched actin filaments by protecting the barbed end from capping (Bear et al., 2002; Hansen and Mullins, 2010; Winkelman et al., 2014). Although filopodia are assumed to play key roles in sensing and transducing guidance signals important for proper growth cone navigation (Bentley and Toroian-Raymond, 1986; Chien et al., 1993; Mattila and Lappalainen, 2008; Dent et al., 2011), their exact role in this process, as well as how guidance cues regulate filopodia formation and dynamics, are poorly understood.

Dorsal root ganglia (DRG) are sensory neurons that extend axon branches distally to the periphery and centrally into the spinal cord dorsal horn. DRG central projections enter the spinal cord at the dorsal root entry zone (DREZ), where they bifurcate and extend branches along the rostral–caudal axis (see Fig. 7 A). The abrupt change in axon orientation requires Slit1 and Slit2, ligands concentrated in the spinal cord midline that repel DRG axons expressing two of their cognate receptors, Robo1 and Robo2 (Kidd et al., 1998, 1999; Fricke et al., 2001; Hao et al., 2001; Long et al., 2004; Ma and Tessier-Lavigne, 2007). In vitro, stimulation of DRG neurons with Slit elicits a rapid reduction in growth cone area termed "collapse" caused, in large part, by actin depolymerization (Gallo and Letourneau, 2004). Repulsive growth cone turning is widely assumed to arise from localized actin depolymerization on the side of the growth cone exposed to the repulsive guidance cue (Lowery and Van Vactor, 2009; Dent et al., 2011; Vitriol and Zheng, 2012). Somewhat paradoxically, data from invertebrate models have demonstrated that Robo-dependent repulsion is mediated in part through Ena/VASP proteins (Bashaw et al., 2000; Yu et al., 2002), which promote actin polymerization (Bear and Gertler, 2009); however, how Slit-Robo signaling affects Ena/VASP-dependent actin assembly and membrane protrusion to enable axon repulsion from Slit remains unclear.

We investigated growth cone dynamics during Slit-Robo–mediated axonal repulsion. We find that axonal repulsion requires the asymmetric formation and extension of filopodia

Correspondence to Frank Gertler: fgertler@mit.edu

A.V. Kwiatkowski's present address is Dept. of Cell Biology, University of Pittsburgh School of Medicine, Pittsburgh, PA 15261.

Abbreviations used in this paper: CC, conserved cytoplasmic motif; CD, cytochalasin D; CU, collapsing units; DIC, differential interference contrast; DRG, dorsal root ganglion; DREZ, dorsal root entry zone; E, embryonic day; HGF, hepatocyte growth factor; mve, mena-vasp-evl null; OBH, oval bundle of His; Sema3A, semaphorin 3A.

Supplemental Material can be found at:
/content/suppl/2016/04/14/jcb.201509062.DC1.html

The Rockefeller University Press $30.00
J. Cell Biol. Vol. 213 No. 2 261–274
www.jcb.org/cgi/doi/10.1083/jcb.201509062

Published April 18, 2016

toward sources of the repulsive guidance cue Slit. Filopodium dynamics are regulated by formation of Robo:Ena–VASP complexes that are formed in response to Slit. DRG sensory afferents lacking all three Ena–VASP paralogs exhibit aberrant invasion of the spinal cord dorsal midline, a phenotype reminiscent of the defects observed in mouse embryos lacking SLIT1/2 or ROBO1/2 (Ma and Tessier-Lavigne, 2007). Although enhanced actin polymerization toward attractive guidance cues is well documented (Shekarabi and Kennedy, 2002; Lebrand et al., 2004; Tang and Kalil, 2005), these data demonstrate that, surprisingly, filopodia assemble and elongate toward the repulsive guidance cue Slit through the interaction of the Robo receptor with Ena–VASP proteins and that this dynamic regulation of filopodia is required for subsequent axonal repulsion.

Results

Slit stimulates elongation of DRG growth cone filopodia

We imaged growth cones on axons extending from organotypic DRG explants by time-lapse microscopy to characterize their responses to Semaphorin3A (Sema3A) and Slit, two established repulsive guidance cues for DRG axons. Application of either Sema3A or the amino-terminal fragment of Slit2 (Slit), which contains the domain responsible for binding to Robo1 and Robo2 (Chédotal, 2007), caused a decrease in the area of lamellipodium veils (termed growth cone collapse; Figs. 1 A and 4 B), consistent with previous studies (Luo et al., 1993; Ma and Tessier-Lavigne, 2007). However, we were surprised to observe that Slit also triggered a rapid (within ∼2 min) elongation of filopodium-like protrusions that were not observed after application of Sema3A (Fig. 1 and Video 1). To determine if filopodium elongation was dependent on ligand concentration, we compared the response of DRG growth cones to Sema3A or Slit over a range of concentrations that induce varying degrees of growth cone collapse (Fig. 1 A). Increasing concentrations of Slit progressively increased the mean length of filopodia, whereas no increases in filopodium length were observed after treatment with Sema3A at any of the concentrations tested (Fig. 1 A). Correlative live-cell and immunofluorescence microscopy revealed that F-actin bundles extend the entire length of the Slit-elicited protrusions, and Mena, a canonical marker of filopodial tip complexes, is found at the distal protrusion ends (Fig. 1 B, arrowheads; and Video 3). Together, these data reveal that Slit, but not Sema3A, elicits elongation of bona fide filopodia from axonal growth cones in organotypic DRG explant cultures.

We reasoned that Slit could induce filopodium elongation by stimulating faster filopodium elongation, increasing the elongation period, or both. Filopodium elongation was characterized by measuring maximum lengths and lifetimes, as well as the rates and periods of extension (Fig. 1 C). We found that filopodia extended from the edge of the growth cone at uniform rates both in unstimulated (59 ± 3 nm/s) and Slit-stimulated conditions (63 ± 3 nm/s; Fig. 1 C), similar to previously reported values for DRG filopodia (Bray and Chapman, 1985). However, Slit increased the elongation period by approximately threefold (105 ± 34 vs. 34 ± 22 s; $P < 0.0001$), resulting in increased filopodium lifetimes and lengths (Fig. 1 C). Thus, Slit-induced filopodium elongation arises from a normal rate of extension that lasts for a longer period of time than observed in unstimulated, spontaneously elongating filopodia.

Filopodia form and elongate toward sources of Slit

The elongation of filopodia in response to a repulsive guidance cue (Fig. 1) lead us to wonder if growth cones encountering gradients of Slit would show directional filopodial responses. We used a micropipette to generate gradients that were essentially linear at a distance 100 µm from the tip of the micropipette (Fig. S1; Pujic et al., 2008) to assay the effects of Slit gradients on axons extending from organotypic DRG explants. When a micropipette was positioned 100 µm from growth cones at a 45° angle, a mock gradient had no effect on filopodium orientation; filopodia were largely distributed evenly around the growth cone periphery, excluding the region occupied by the axon (Fig. 2 A). However, exposure to a Slit gradient produced a clear increase in the proportion of filopodia on the growth cone quadrant proximal to the higher Slit concentration (Fig. 2 A). This change in the orientation of filopodia toward the Slit gradient was caused by an increase in the number of filopodia facing the gradient, whereas the number of filopodia distal to the gradient remained essentially unchanged (Fig. 2 B). The increase in the number of filopodia was accompanied by a lengthening of filopodia proximal to the gradient: proximal filopodia were 37% longer after Slit exposure (10.5 ± 5.4 vs. 7.7 ± 3.6 µm) and were 17% longer than those on the distal growth cone quadrant, which were exposed to lower Slit concentrations (Fig. 2 C and Fig. S1). These data indicate that, in DRG explants, axonal growth cones encountering a spatially asymmetric Slit gradient respond by forming and elongating filopodia toward, rather than away from, higher concentrations of Slit.

Regulated filopodia dynamics are required for Slit chemorepulsion

The finding that filopodia extend toward a source of Slit was surprising, because it has conventionally been thought that repulsive guidance cues such as Slit mainly induce bulk actin depolymerization (Dent et al., 2011; Vitriol and Zheng, 2012). Therefore, we tracked growth cone trajectories to confirm that axons were in fact repelled by the Slit gradients, as would be expected. Growth cones in a mock gradient grew outward in a random distribution within ±45° from the median (Fig. 2 D). Application of a Slit gradient induced a net repulsion of axons (−9 ± 2° turning angle) compared with controls (0 ± 2°), with few "attractive" movements toward the micropipette (Fig. 2 E).

We next asked if Slit-mediated filopodium formation and elongation is required for axon repulsion. We measured the response of neurons in organotypic DRG explants isolated from embryos lacking all three Ena–VASP paralogs (Mena, VASP, and EVL; triple null is referred to hereafter as mve). When cultured in vitro, mve DRG growth cones are almost completely devoid of filopodia (Fig. 2 D, iv), consistent with previously published phenotypes of cortical neurons (Dent et al., 2007; Kwiatkowski et al., 2007) and fibroblasts (Bear et al., 2000; Mejillano et al., 2004) that lack Ena–VASP. When exposed to a Slit gradient, mve axons exhibited directionally persistent forward movement without deflecting away from Slit (Fig. 2 D). However, this defective response to Slit could be caused by loss of Ena–VASP function that is not directly related to filopodia. To determine if inhibiting filopodium dynamics in wild-type neurons would affect the turning response, we treated neurons

Published April 18, 2016

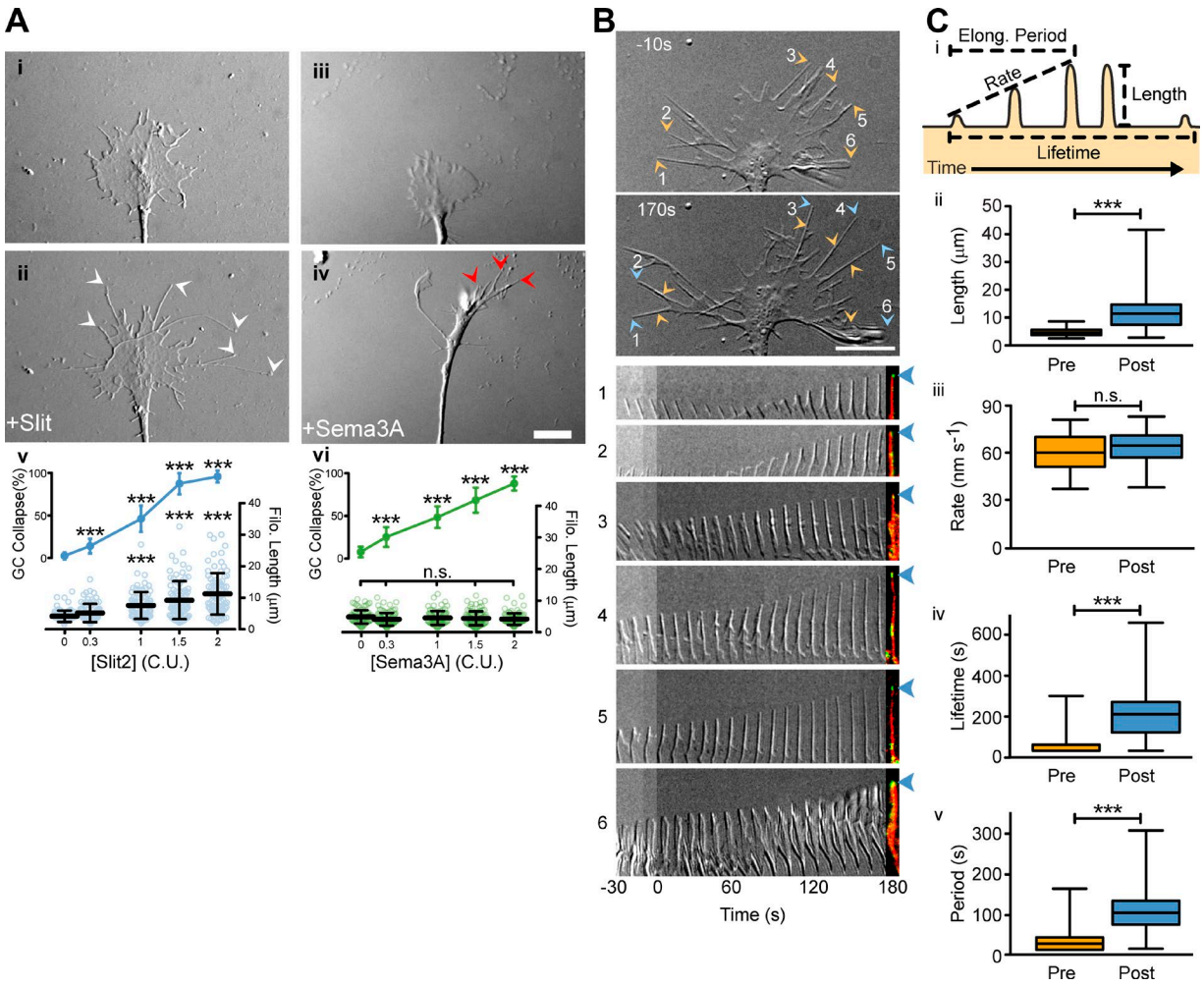

Figure 1. **Slit induces filopodium elongation.** (A) DIC images of DRG growth cones 15 s before (i and iii) and 10 min after addition of 1.5 collapsing units (CU) of either Slit (ii) or Sema3A (iv). One CU is the ligand concentration which induces ~50% growth cone collapse (Slit2, 400 ng/ml; Sema3A, 500 ng/ml). Note the elongation of filopodia after stimulation with Slit (ii, white arrowheads mark filopodium tips), but not with Sema3A (iv, red arrowheads mark retraction fibers). See Videos 1 and 2. Growth cone collapse (solid lines) and filopodium length were measured over a concentration range of Slit2 (v, blue) or Sema3A (vi, green); for ease of comparison, concentrations are given as CU. Greater than 40 growth cones were scored at each concentration per condition. ***, $P < 0.0001$; n.s., $P > 0.05$; one-way ANOVA. (B) Live-cell DIC images of a growth cone during stimulation with 1.5 CU Slit. Filopodium tips are marked at 10s before (orange arrowheads) and at 170s after (blue arrowheads) Slit stimulation. Montages show time-lapse images of single filopodia, with the far-right panel showing an immunofluorescent image of the same filopodium after fixation at 180s post-Slit (phalloidin [F-actin], red; Mena, green). See Video 3. Bars, 10 µm. (C) Spontaneous and Slit-induced filopodium elongation (Elong.) kinetics were measured from DIC images captured every 5 s for 10 min before and after Slit addition. (i) Depicts length, rate, lifetime, and extension period measurements shown in panels ii–v (ii–v: preslit, $n = 638$ filopodia; postslit, $n = 560$ filopodia; 15 biological replicates). ***, $P < 0.0001$; n.s., $P > 0.05$; two-tailed t test.

with cytochalasin D (CD), which caps the barbed ends of actin filaments in a stochastic manner at low concentrations (25 nM) known to inhibit filopodia without disrupting lamellipodia (Dent et al., 2007; Hansen and Mullins, 2015). Strikingly, wild-type neurons treated with CD at the onset of the Slit gradient failed to deflect away from Slit, essentially phenocopying the response of mve axons (Fig. 2 D). Thus, blocking the dynamic and spatially oriented formation and elongation of filopodia is sufficient to inhibit repulsive movement of DRG growth cones away from Slit.

Regulated filopodia dynamics are required for Slit-induced axon retraction

We noticed that exposing growth cones to high concentration Slit gradients, either by positioning the micropipette close to the axon or by loading a high concentration of Slit in the micropipette, could cause growth cone collapse followed by axon retraction (Fig. S3). Intriguingly, we never observed retraction in mve axons; however, as it was technically difficult to elicit this response reproducibly in controls, we sought a more reliable method of examining axon retraction. Bath application of Slit to control DRG neurons caused growth cone collapse (Fig. 3, A and B; and Video 4) and axon retraction in a dose-dependent manner: few axons retract at low (1 nM) Slit concentrations, whereas concentrations of Slit 4.5 nM or higher caused uniform axon retraction (Fig. 3 C). Although increasing concentrations of Slit progressively diminished the rate of mve axon extension, retraction of mve axons was never observed, even at the highest Slit concentration tested (30 nM; Fig. 3 C and Video 5; unpublished data). Indeed, some mve axons continued to extend even after stimulation with 6 nM Slit, a concentration that universally evoked retraction in controls (Fig. 3 C). Similarly, acute inhibition of filopodium dynamics with CD blocked axon retraction normally elicited by 6 nM Slit (Fig. 3 D). Although

Published April 18, 2016

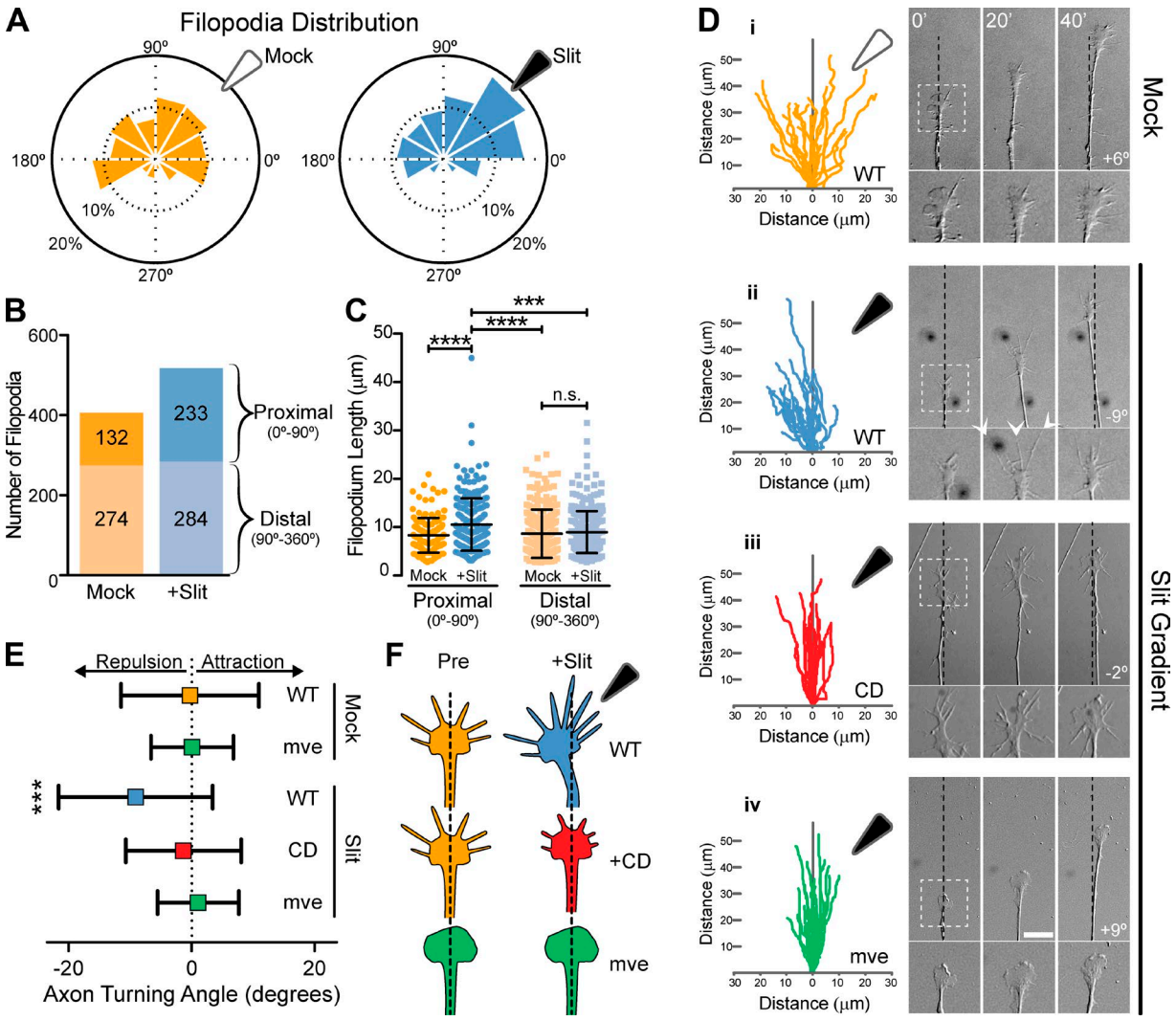

Figure 2. **Extension of filopodia toward sources of Slit is required for axon repulsion.** (A) Polar histogram plots of filopodium distribution. Data were quantified from DIC images taken over a 10-min period after application of the indicated gradient; orientation of micropipette-generated gradients indicated by black triangle (open, mock; filled, Slit). Data are binned from six independent experiments examining a total of 24 growth cones. (B) Numbers of filopodia on the side of the growth cone facing toward (darker shades, proximal, 0–90°) or away from (lighter shades, distal, 90–360°) the Slit gradient. (C) Lengths of filopodia by relative orientation to mock (orange) or Slit (blue) gradients. Filopodia proximal to the Slit gradient were significantly longer (10.5 ± 5.4 µm) than filopodia exposed to a mock gradient (7.7 ± 3.6 µm) or filopodia distal to the gradient (8.9 ± 4.3 µm). ***, $P < 0.001$; ****, $P < 0.0001$; n.s., not significant; one-way ANOVA. (D) Traces of growth cone positions over a 30-min period after application of mock or Slit gradients. Representative DIC images show axons just before gradient application (0′) and after 20 or 40 min; insets show higher magnification views of growth cones at the corresponding time points. A total of 25 nM CD was added to the bath media at the time of the gradient onset in iii. Long filopodia were frequently observed in Slit gradients applied to control (ii, white arrowheads), but not in CD-treated (iii) or mve neurons (iv). (E) Axon turning angles in response to gradients (mean ± SD). $n \geq 18$ biological replicates for each condition. ***, $P < 0.001$; one-way ANOVA. (F) Summary of relationships between filopodia extension toward sources of Slit and axon repulsion. Bars, 10 µm. WT, wild type.

inhibiting filopodia with CD or ablating filopodia by genetic removal of Ena–VASP had profound effects on axon retraction, both of these conditions showed no significant differences in Slit-induced reduction in growth cone area compared with controls (Fig. 3, A and B). These data indicate that Robo signals are transduced in the absence of filopodia but that normal axonal responses to Slit require regulated filopodium dynamics.

Slit promotes association of Ena–VASP with Robo

We explored the possibility that Slit-elicited filopodium elongation involved Ena–VASP proteins, which (1) promote actin filament elongation (Bear and Gertler, 2009), (2) are concentrated at the tips of filopodia (Dent et al., 2011), (3) can bind to Robo in vitro (Bashaw et al., 2000; Yu et al., 2002), and (4) remain concentrated at the tips of filopodia undergoing Slit-induced elongation (Fig. 1 B). The *Drosophila melanogaster* orthologs of Robo1 and Mena were shown to exist in biochemical complexes in whole *Drosophila* embryo lysates (Bashaw et al., 2000); however, the cell biological consequences of this interaction, as well as its sensitivity to ligand stimulation, remain unclear. To determine if vertebrate Mena associates with Robo in a Slit-regulated manner, we immunoprecipitated endogenous Robo-1 from neuronal-like CAD cells (Byun et al., 2012). Under basal conditions, Mena was weakly detected in complex with Robo-1; however, Slit treatment induced robust coimmunoprecipitation of Robo–Mena complexes (Fig. 4 A). The increased abundance of Robo–Mena complexes after Slit

Published April 18, 2016

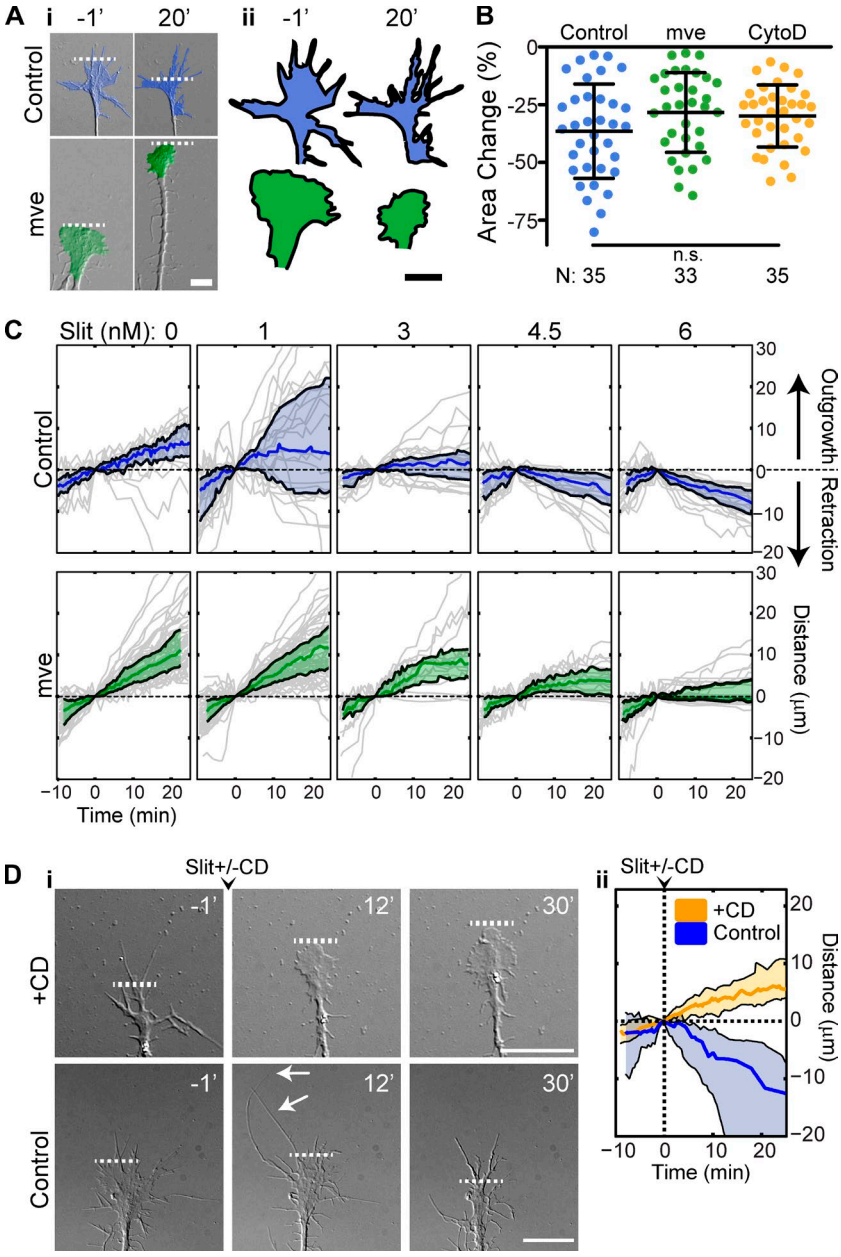

Figure 3. **Slit-induced axon retraction requires regulation of filopodia dynamics.** (A) DIC time-lapse images of littermate control and mve DRG axons 1 min before and 20 min after bath application of 3 nM Slit. The distal-most leading edge is marked by a white dashed line, and growth cone areas shaded either blue (control) or green (mve) in panel i are enlarged and aligned for easy comparison in ii. (B) Area measurements were generated by manually outlining growth cones just before ligand addition (Apre) and 20 min after stimulation with the indicated ligands (Apost). Fractional change in area is calculated as 1 − (Apre − Apost)/Apre. Negative values indicate a decrease in growth cone area. (C) Growth cone position tracked from time-lapse DIC images; traces normalized so that the origin corresponds to growth cone position at the time of Slit stimulation (colored line, mean; shaded area, 95% confidence interval). $n \geq 18$ for each condition. (D) DRG neurons stimulated with 5 nM Slit and either 25 nM CD or DMSO (control). Slit-induced filopodium elongation is observed in controls (i, white arrows), but not in CD-treated growth cones. CD blocks Slit-induced axon retraction; compare positions of growth cone leading edge (dashed lines in i) and growth cone position (ii, tracked as in C). Bars, 10 µm. $n = 18$ for each condition.

application occurred on a similar timescale as filopodium elongation (Figs. 1 and 2), consistent with the notion that dynamic regulation of Robo–Mena complex formation might regulate the increase in filopodium number and length in response to Slit.

We explored this interaction further by pull-down assays of GFP-tagged fragments of rat Robo1 using immobilized recombinant mouse Ena–VASP homology 1 (EVH1) domain, which mediates protein–protein interactions with several Ena–VASP binding partners (Niebuhr et al., 1997; Peterson and Volkman, 2009). We observe a robust interaction between EVH1 and a segment of Robo containing the Conserved Cytoplasmic 2 (CC2) motif (Fig. 4 C, asterisk), which includes a canonical EVH1 binding site (F/L followed by four prolines, abbreviated as LP4; Niebuhr et al., 1997) previously identified in Drosophila Robo1 (Bashaw et al., 2000). This interaction was dependent on the LP4 sequence, as a leucine-to-alanine substitution disrupted EVH1 binding ($CC2^{m}$; Fig. 4 D). Interestingly, we found that the near-full-length Robo intracellular domain showed no binding to EVH1, despite containing CC2 (Fig. 4 C). Indeed, EVH1 binding was inversely correlated with the length of the construct containing CC2 (Fig. 4 E). We reasoned that EVH1 binding sites might be obscured in the context of the full-length protein in the absence of ligand and that ligand binding could relieve this putative autoinhibition. If this were the case, it would be possible that other EVH1 binding sites existed within the Robo intracellular domain that would not be detected using our pull-down approach; we therefore probed arrays of overlapping peptides spanning the entire intracellular portion of Robo1 with purified recombinant protein containing the Mena EVH1 domain. This analysis confirmed binding to CC2 and also identified an additional potential binding site in CC3 (Fig. S2 A). Sequence analysis revealed that although the LP4 motif in CC2 is highly conserved evolutionarily, the CC3 LP4 motif exhibits considerably less conservation among Robo family members and homologs (Fig. S2 B) and showed no interaction with EVH1 in our pull-down assays (Fig. 4 C).

Published April 18, 2016

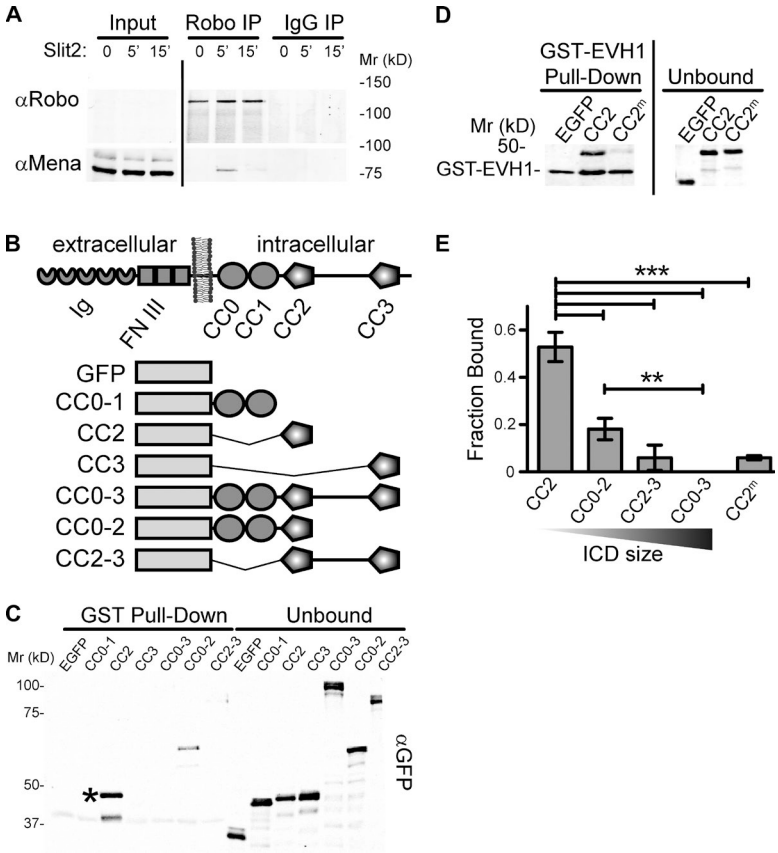

Figure 4. **Slit regulates filopodium dynamics by inducing a direct interaction between Mena EVH1 and Robo CC2.** (A) Western blots of anti-Robo1 immunoprecipitates (IP) from CAD cells after stimulation with 5 nM Slit at the indicated times. Robo1 was not detectable in the unenriched input fraction. (B) Domain diagrams of Robo1/2 and Robo1-derived constructs used for pull-down experiments. (C) GST-EVH1 was used to pull down GFP-tagged fragments of the Robo intracellular domain from HEK293 cell lysates; robust interaction was detected with GFP-CC2 (asterisk). (D) GST-EVH1 pull-down from lysates of HEK293 cells expressing GFP-CC2 or GFP-CC2 in which the EVH1 binding site was mutated (CC2m, L>A substitution). Pull-down and unbound fractions displayed are from the same Western blot exposure; irrelevant lanes have been removed for clarity. (E) Densitometric analysis of GST-EVH1 pull-down of Robo intracellular domain (ICD) fragments containing the CC2 motif (mean ± SD, three independent experiments). **, $P < 0.001$; ***, $P < 0.0001$.

Together, these data support a model in which Slit induces a conformational change in Robo that is required for robust binding of CC2 to the EVH1 domains of Ena–VASP proteins.

Ena–VASP binding to Robo CC2 is required for ligand-induced filopodium elongation

To determine whether Slit-induced filopodium elongation requires direct interaction of Mena with Robo, we tested if disrupting EVH1 binding sites in the intracellular domain of Robo affected growth cone responses. To facilitate analysis of Robo mutants, we used a previously developed chimeric receptor in which the extracellular portion of the hepatocyte growth factor (HGF) receptor, Met, is fused to the transmembrane and intracellular sequence of Robo1; upon stimulation with HGF, Met-Robo transduces repulsive signals normally elicited by Slit without activating endogenous Robo receptors (Stein and Tessier-Lavigne, 2001). For these experiments, constructs were cotransfected with a GFP reporter into primary cultures of dissociated DRG neurons. Filopodia in Met-Robo–expressing neurons appeared similar to GFP-transfected controls in number, length, and dynamics and displayed normal responses when stimulated by Slit (robust filopodium elongation and decreases in growth cone area; Fig. 5, B and C). Upon stimulation with 50 ng/ml HGF, Met-Robo–expressing growth cones exhibited filopodium elongation similar to that elicited by Slit (Fig. 5 B). GFP-transfected DRG neurons show no apparent response to HGF, indicating that HGF stimulates filopodium dynamics solely through the expressed Met-Robo chimaera (Fig. 5, A and B). Interestingly, mutation of the EVH1 binding site in CC2 ($CC2^m$) of the Met-Robo chimera completely disrupted filopodium elongation elicited by HGF, whereas an analogous mutation in CC3 ($CC3^m$) did not interfere with HGF-elicited filopodium elongation (Fig. 5 B). HGF stimulation of any of the Met-Robo chimera–transfected (MR, $CC2^m$, or $CC3^m$) neurons resulted in decreases in growth cone area (~50%) similar to what is typically seen after stimulation with Slit (Fig. 5 C). These data indicate that all the chimeric receptors tested were capable of mediating some ligand responses and that lamellipodium dynamics can be regulated independently of filopodia. Thus, a functional Ena–VASP binding site in CC2 is dispensable for the regulation of lamellipodia but is required for the induced elongation of growth cone filopodia after activation of the Robo receptor.

Robo requires a functional Ena–VASP binding site in CC2 to mediate axonal repulsion

The finding that the Ena–VASP binding site in the Robo CC2 motif was required for filopodium elongation, but dispensable for growth cone collapse (Fig. 5), allowed us to determine if these activities are required for axonal repulsion. We transfected Met-Robo chimeras or a GFP control into wild-type DRG neurons and examined the response of filopodia (length and number) and axon turning to a gradient of HGF. As expected, we saw no response to HGF in the GFP-transfected controls (Fig. 6). Similar to wild-type neurons responding to a Slit gradient (Fig. 2), we observed an increase in the number of filopodia oriented toward the HGF gradient in Met-Robo transfected growth cones (Fig. 6 A; 0–45°). Additionally, a ~30% increase in filopodium length was observed after the onset of the HGF gradient only in the Met-Robo–transfected growth cones (before, 5.7 ± 2.7 µm; after, 7.4 ± 4.5 µm; Fig. 6 B). Again, similar to filopodia in a Slit gradient (Fig. 2), the filopodia proximal to the HGF gradient showed a stronger response

Published April 18, 2016

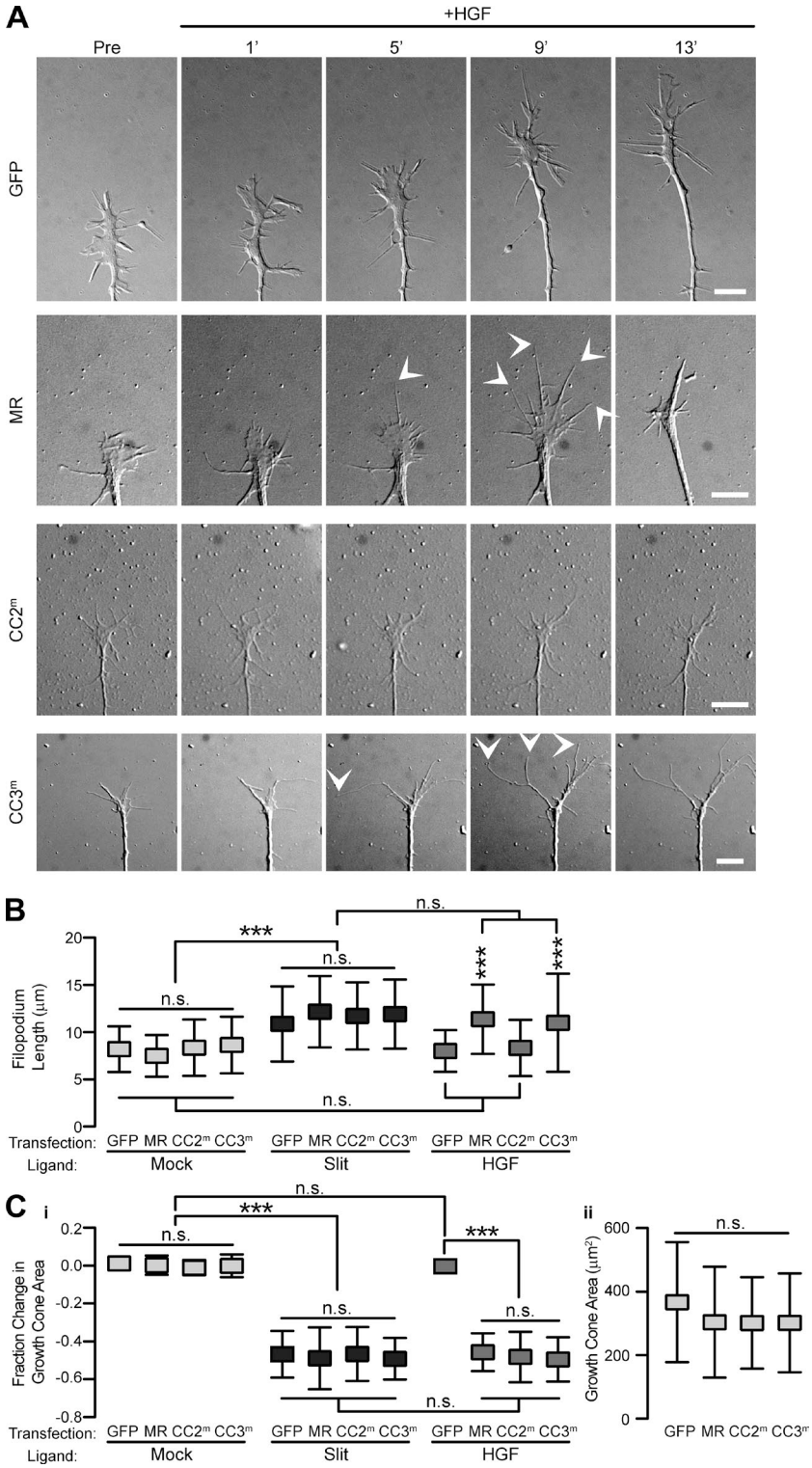

Figure 5. **Robo-mediated filopodium elongation requires a functional Ena–VASP binding site.** (A) DRG neurons were transfected with the indicated constructs and stimulated with 100 ng/ml HGF. White arrowheads mark extremely long filopodia observed after HGF stimulation in growth cones expressing Met-Robo or CC3m. Bars, 10 µm. (B) DRG neurons were transfected with the indicated constructs and stimulated with the indicated ligands at time 0. The maximum length of individual filopodia were measured during a 10-min period starting 5 min after ligand addition. Activation of endogenous Robo by Slit elicited similar filopodium elongation in all conditions. (C) Area measurements were generated by manually outlining growth cones just before ligand addition (Apre) and 20 min after stimulation with the indicated ligands (Apost). Fractional change in area (i) is calculated as −(Apre − Apost)/Apre. Negative values indicate a decrease in growth cone area. (ii) Raw growth cone area values. ***, $P < 0.0001$; n.s., not significant (mean ± SD, one-way ANOVA, $n \geq 6$ biological replicates for all conditions).

in Met-Robo–expressing growth cones than those located distal to the gradient (Fig. 6 C). However, growth cones transfected with the $CC2^m$ construct actually exhibited a slight decrease in the number of filopodia both proximal and distal to the HGF gradient (Fig. 6 A). Additionally, mutation of the Ena–VASP binding site in CC2 abrogated the ligand-induced increase in filopodium length evoked in the Met-Robo–expressing growth cones (Fig. 6, B and C). Importantly, axonal repulsion away from the HGF gradient in the Met-Robo–expressing neurons (−18.5 ± 15.7°) was not observed in either GFP controls (0.2 ± 13.8°) or in neurons expressing $CC2^m$ (4.8 ± 16.6°) (Fig. 6 D). Together, these data indicate that the Ena–VASP binding site in the Robo CC2 motif is required to mediate both the spatially oriented formation and elongation of filopodia toward a repulsive ligand (Fig. 6, A–C) and the eventual movement of the axon away from the source of the repulsive cue (Fig. 6 D).

Published April 18, 2016

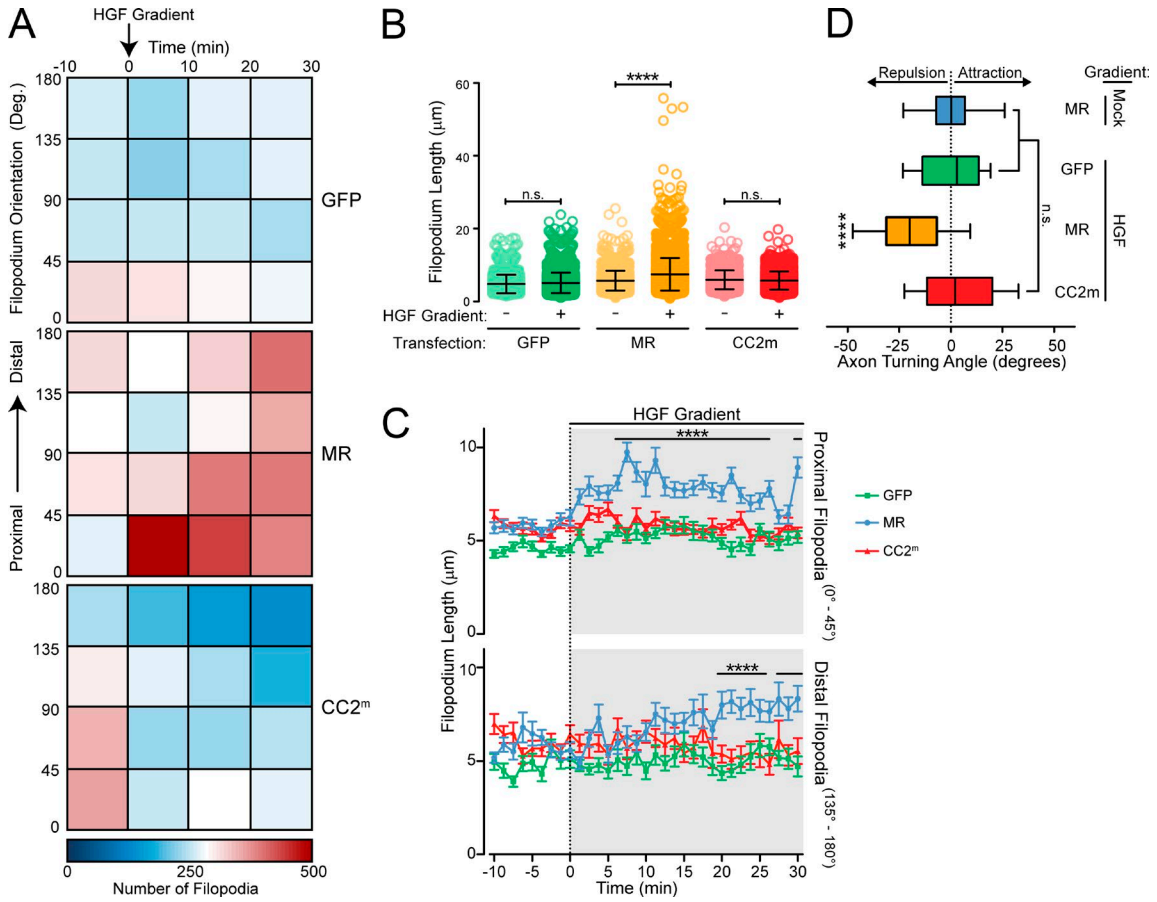

Figure 6. **A functional Ena–VASP binding site in CC2 is required to mediate axon repulsion downstream of Robo activation.** (A) Heatmaps showing the distribution of growth cone filopodia relative to an HGF gradient over time. HGF gradient was started at time 0; filopodia within 0–45° are nearest the pipette. Color scale indicates the number of filopodia. *n* = 18 growth cones per condition. (B) Lengths of all filopodia scored before (–) and after (+) onset of HGF gradient. Black lines, mean ± SD; *n* = 13,727 filopodia. (C) Length of filopodia nearest (proximal, top) and furthest (distal, bottom) from the HGF gradient over time. Mean ± SEM. Black bars denote points where MR was significantly different from GFP and CC2m ($P < 0.001$). (D) Box and whisker plots of axon turning angles in response to the indicated gradients. *n* = 18 growth cones per condition. n.s., $P > 0.05$; ****, $P < 0.0001$; one-way ANOVA.

Abnormal DRG axon extension toward the dorsal midline by mve axons in vivo

Perturbing filopodia or the interaction of Robo with Ena–VASP proteins produced severe defects in Robo-mediated axon guidance in our in vitro assays, prompting us to examine DRG axon guidance in mve embryos (Fig. 7). To confirm that mve growth cones lack filopodia in vivo, spinal cord explants cultured ex vivo were infected with herpes simplex virus encoding soluble tdTomato. Using this approach, we could clearly trace axonal projections from the DRG and readily observed filopodia on control growth cones inside the DREZ but failed to detect filopodia on mve growth cones (Fig. 7 B).

We performed whole-mount immunofluorescence on fixed embryos to examine axon tracts; horizontal optical sections across the spinal column at the level of the DREZ (Fig. 7 A, gray plane) clearly showed that DRG central projections in embryonic day 10.5 (E10.5) control embryos had made the rostral–caudal turn and formed a prominent lateral axon tract called the oval bundle of His (OBH; Fig. 7, C and D). However, mve embryos exhibited a severely disrupted axonal organization, with DRG central projections aberrantly extending toward the dorsal midline and failing to form a recognizable OBH at E10.5 (Fig. 7, C and D). Although lateral axon tracts formed in mve embryos by E12.5 (Fig. 7 C), the OBH appeared broad and loosely fasciculated (Fig. 7, C and D, compare areas outlined with red dashed lines). Additionally, neurofilament-positive axons could be observed invading the dorsal midline in mve embryos, but not in littermate controls (Fig. 7, C and E; and Fig. S4). Indeed, axons in mve embryos could be observed extending nearly to the posterior median septum and were tipped by growth cones appearing to lack discernible filopodia (Fig. 7 C, vii). The failure of mve axons to properly orient in the DREZ at E10.5, and the aberrant invasion of axons into the dorsal midline at E12.5 (Fig. 7 and Fig. S4), are similar to defects observed for DRG axons in the DREZ of embryos lacking either Slit or Robo (Ma and Tessier-Lavigne, 2007). Consistent with our earlier study implicating Ena–VASP function downstream of Netrin (Lebrand et al., 2004), we also observed evident defects in commissural axon crossing in the ventral midline of mve embryos compared with littermate controls (TAG-1 positive axons; Fig. S4 C). Together, these findings suggest that Ena–VASP proteins are required for proper responses to Slit–Robo signaling in vivo, mirroring the results of our in vitro assays.

Discussion

We conclude that the repulsive guidance cue Slit induces both the formation of DRG growth cone filopodia, as well as a rapid, robust elongation of filopodia, by promoting formation

Published April 18, 2016

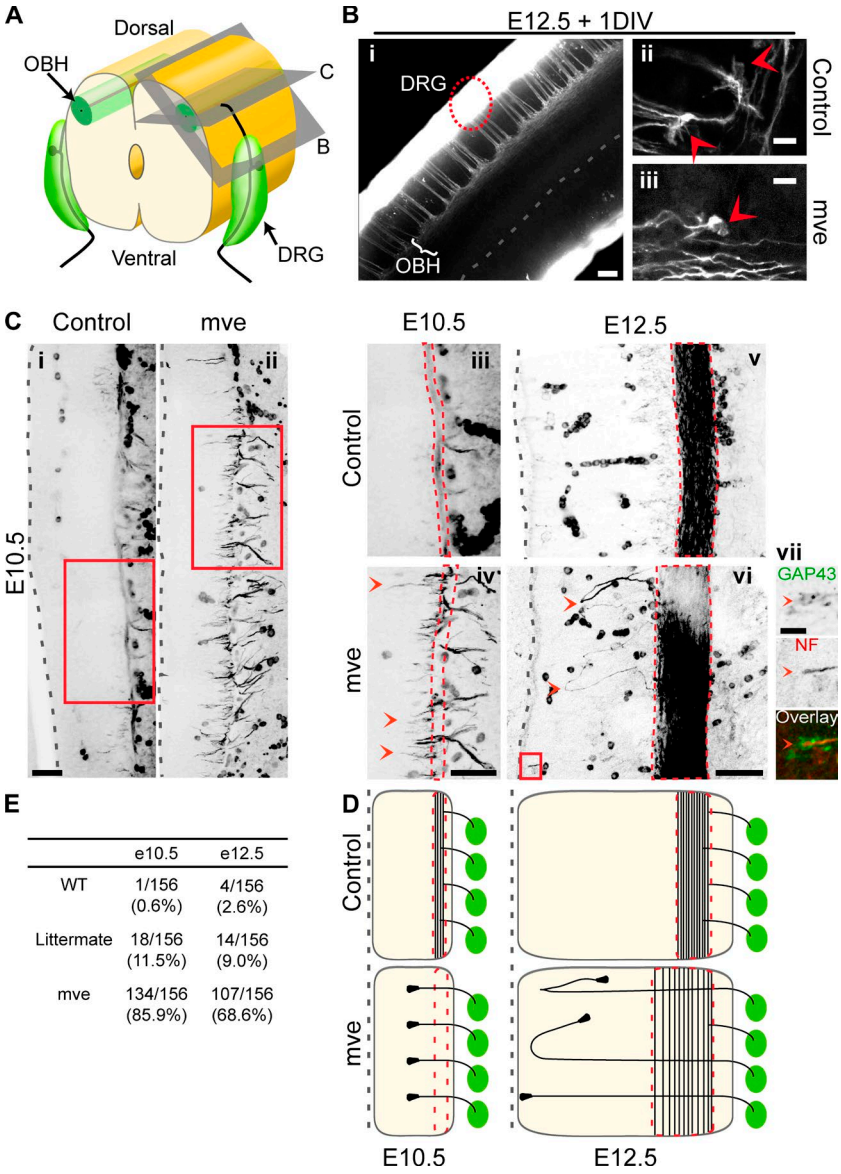

Figure 7. **DRG axon guidance defects in mve mutant embryos.** (A) Diagram of DRG projections in an embryonic spinal cord. Gray planes indicate the orientation and location of optical sections shown in B and C. (B) Confocal images of spinal cord explants infected with HSV-tdTomato to visualize DRG projections. Filopodia are observed on growth cones in control, but not mve, embryos (compare growth cones marked by red arrowheads in ii and iii). (C) Confocal micrographs of whole-mount embryos stained with neurofilament antibody to label axons. Only the right half of the spinal cord is shown for clarity. Boxed areas in i and ii are enlarged in iii and iv. OBH is outlined in red dashed lines in C and D. Boxed region in vi is enlarged in vii, revealing a growth cone lacking filopodia near the ventral midline. (D) Schema of axonal projection patterns observed in control and mve embryos at E10.5 and E12.5. (E) Quantification of central projection defects in wild-type (m+/+v+/+e+/+), littermate ((m+/+v−/−e−/−)/(m+/−v−/−e−/−)), and Ena/VASP null (m−/−v−/−e−/−) embryos. Thoracic spinal levels in six embryos (corresponding to 156 DRG) were scored for each condition; a spinal level was scored as defective if no recognizable OBH was present (C, iv) or if NF-positive axons extend past the OBH toward the dorsal midline (C, vi). Bars: (B, i–iii; and C, i–vi) 50 µm; (C, vii) 10 µm. GAP43, growth associated protein 43; NF, neurofilament; DIV, days in vitro; WT, wild type. Circular objects in C are autofluorescent cells.

of complexes containing the Robo receptor and Ena–VASP proteins. Filopodia preferentially form and elongate toward Slit gradients, and genetically or pharmacologically disrupting filopodium formation or dynamics blocks repulsion away from Slit sources. In vivo, we find that Ena–VASP–deficient growth cones, which lack discernible filopodia, are unable to accomplish the rostral–caudal turn normally made by DRG axons as they enter the DREZ around E10.5, similar to defects observed in embryos lacking either Slit (Slit 1/2$^{-/-}$) or Robo (Robo 1/2$^{-/-}$; Ma and Tessier-Lavigne, 2007).

Despite the established dosage-sensitive genetic interactions between mutations in the Robo and Ena–VASP homologs in *Drosophila* and *Caenorhabditis elegans*, complete loss of Ena–VASP proteins produces only mild midline axon guidance phenotypes in these invertebrate model systems (Bashaw et al., 2000; Yu et al., 2002) compared with what we observe in mve mice (Fig. 7). These findings suggest either that Ena–VASP–regulated filopodium dynamics play expanded or additional roles in axon guidance in vertebrates or, alternatively, that invertebrates use Ena–VASP–independent mechanisms not present in vertebrates. Given the increased size and complexity of the vertebrate nervous system and the other significant differences in how Robo is regulated in vertebrates and invertebrates (Keleman et al., 2002; Chen et al., 2008; Colak et al., 2013; Zelina et al., 2014), it is not surprising that other aspects of this pathway have also diverged.

Actin dynamics in repulsive axon guidance

A common model for axon guidance proposed by many laboratories (including our own) posited that growth cone turning is initiated by opposing actions of attractive and repulsive guidance cues on the actin cytoskeleton: attractive cues promote actin polymerization, whereas repulsive cues cause proximal actin filament disassembly (Dent et al., 2011; Vitriol and Zheng, 2012). This model is intuitively appealing and is based on strong experimental evidence showing that attractive cues promote actin polymerization (Shekarabi and Kennedy, 2002; Lebrand et al., 2004; Tang and Kalil, 2005; Marsick et al., 2010), whereas bath application of repulsive cues induce actin disassembly and growth cone collapse (Raper and Kapfhammer, 1990; Cox et al., 1990; Luo et al., 1993; Fan et al., 1993; Brose et al., 1999; Nguyen Ba-Charvet et al., 1999; Niclou et

Published April 18, 2016

al., 2000; Ma and Tessier-Lavigne, 2007). One example of this is the Semaphorin family of repulsive guidance cues: when applied to the bath media of neurons in culture, Sema3A induces total growth cone collapse in which both the lamellipodia and filopodia disassemble (Luo et al., 1993; Fig. 1). A series of elegant genetic and biochemical approaches revealed that Semaphorin-induced F-actin disassembly is mediated through redox regulation of actin by the enzyme Mical (Terman et al., 2002; Hung et al., 2010, 2011). Interestingly, earlier work showed that contact of a growth cone filopodium with a Semaphorin-coated bead induces local disassembly of lamellipodia adjacent to the contacting filopodium, with an anticorrelated increase in lamellipodial protrusion on the contralateral side of the growth cone that produces growth cone turning (Fan and Raper, 1995). Like Semaphorin, Slit-mediated repulsion involves inhibiting lamellipodia (Fig. 5); however, Slit also promotes filopodia, an activity not seen for Sema3A (Fig. 1). This difference demonstrates that axon repulsion can be orchestrated via distinct types of cytoskeleton-mediated morphodynamics that ultimately lead to a suppression of lamellipodial extension or to lamellipodial retraction. Using different mechanisms to mediate axon turning may offer neurons another level of regulation to further differentiate or fine-tune responses to combinations of different guidance signals.

Our data suggest that activation of Robo acts as a kind of molecular switch that promotes the elongation of filopodia while concomittantly inhibiting lamellipodia. At a molecular level, Robo could accomplish this by promoting addition of actin monomers onto the free barbed ends of existing actin filaments through association with Ena–VASP proteins (Bashaw et al., 2000; Fig. 5) while simultaneously inhibiting branched actin networks through association with GTPase activating proteins that inhibit Arp2/3-mediated nucleation (SRGAP1 and CrGAP–Vilse; Wong et al., 2001; Lundström et al., 2004; Hu et al., 2005). The net effect of this would be to shunt actin polymerization toward long, unbranched actin filaments (e.g., filopodia) at the expense of branched actin networks (e.g., lamellipodia). Current models of F-actin network regulation (Carlier and Pantaloni, 1997; Akin and Mullins, 2008) suggest that actin filaments essentially compete for a limited pool of available actin monomers to continue polymerizing. A consequence of these models is that factors that suppress one type of actin network may conversely promote the polymerization of other actin-based structures by increasing the available pool of monomeric actin. This conceptual framework suggests that Slit-induced disassembly of growth cone lamellipodia (Fig. 3, A and B) should increase the actin monomer concentration and could therefore contribute to or directly cause filopodium formation and elongation (Fig. 1). However, increased actin monomer concentration by itself does not appear to be sufficient to support ligand-induced filopodium elongation: mutation of the Ena–VASP binding site in Robo does not impair ligand-induced lamellipodium disassembly, but it does disrupt filopodium elongation (Figs. 5 and 6). Thus, the effects of Robo activation on branched (lamellipodia) and linear (filopodia) actin networks appear to be coordinated yet independent activities mediated by discrete protein–protein interactions with defined regions of the Robo cytoplasmic tail (Figs. 4, 5, and 6).

Filopodia are required for Slit–Robo–mediated axon repulsion

The regulation of lamellipodia and filopodia downstream of Robo appear to be separable activities: neurons expressing a Met-Robo chimera lacking a functional Ena–VASP binding site fail to elongate filopodia in response to ligand yet still exhibit a ligand-dependent decrease in growth cone area (Fig. 5, B and C). Additionally, Slit treatment of growth cones lacking filopodia elicits a robust decrease in growth cone area similar to controls (Fig. 3, A and B). This decrease in growth cone area is one of the primary attributes of "growth cone collapse," a descriptive phrase that is frequently used to describe, and assay for, the repulsive activity of guidance cues (Bray et al., 1980; Kapfhammer et al., 1986; Cox et al., 1990; Piper et al., 2006; Hata et al., 2009; Yue et al., 2013). However, we find that although growth cones lacking filopodia exhibit signs of "collapse" after Slit stimulation, they exhibit marked defects in Slit-elicited axon retraction (Fig. 4, C and D) and axon repulsion (Fig. 2, D–F). Furthermore, disruption of the Robo-Ena–VASP interaction does not affect collapse (Fig. 5 C), but it does block Robo-mediated effects on filopodium length (Fig. 5, A and B; and Fig. 6, A–C) and axonal repulsion (Fig. 6 D). Thus, collapse of the growth cone lamellipodial veil, a process that normally precedes, or occurs concomitantly with axon repulsion, is insufficient for successful Robo-mediated axon guidance in the absence of Slit-elicited changes in filopodium dynamics.

Why would growth cones elaborate filopodia in response to a repulsive guidance cue such as Slit? One potential function for this behavior is that the area a growth cone samples increases with the square of its radius (Gallo and Letourneau, 2004); thus, increasing the number and/or length of filopodia is an efficient way for migrating axons to sample their environment. For example, the filopodium elongation observed toward Slit gradients (~37%; Fig. 2 C) increased the area sampled by growth cones by nearly 70%. In the context of an extracellular gradient, this increase in sampling area effectively magnifies differences between low and high concentrations, potentially enabling better resolution of shallow gradients. This model has been invoked to explain why growth cones become larger and more "complex" (ratio of perimeter/area) at choice points in vivo (Raper et al., 1983; Tosney and Landmesser, 1985; Waxman et al., 1995). In addition to their potential sensory function, filopodia have also been shown to play key roles in forming adhesions to substrates, directing microtubule exploration of the growth cone periphery, serving as organizers of directional endo- and exocytosis, and as sites of localized signaling (Robles et al., 2003; Dent et al., 2011; Ros et al., 2015). It was recently found that in the case of axonal attraction toward Netrin, extension of filopodia toward a Netrin gradient is regulated by changes in VASP monoubiquitination (Menon et al., 2015). Thus, regulation of filopodia by different guidance receptors can use distinct mechanisms that produce disparate outcomes: filopodial extension induced by Slit is required for repulsion, whereas filopodial extension induced by Netrin causes attraction. A key goal of future studies will be to examine how filopodia integrate these diverse cellular processes in defined spatiotemporal patterns in response to extracellular cues to enable proper axon guidance.

Most of our knowledge of how axon guidance cues function comes from genetic or biochemical screens that identified signaling pathway components and downstream effectors; however, relatively few subsequent studies have examined the contribution of these pathways to regulating growth cone cytoskeleton dynamics at high spatial and temporal resolution. The unexpected finding that Slit promotes the formation and extension of DRG filopodia highlights the need for more detailed study of the regulation of cytoskeleton network dynamics by

Published April 18, 2016

axon guidance cues, particularly those that mediate repulsion. Bringing new approaches and technologies to bear on investigating the dynamics of these signaling pathways promises to yield informative and unexpected insight into the mechanisms regulating nervous system development.

Materials and methods

Western blotting

All reagents were obtained from Sigma-Aldrich unless noted otherwise. Protein samples were resolved with SDS-PAGE using 10% gels (Bio-Rad Labortories). For immunoblotting, proteins were transferred to nitrocellulose membranes (80 V, 3 h) at 4°C. Stock solutions of antibodies were diluted 1:1,000 in PBS-T (137 mM NaCl, 7 mM Na_2HPO_4, 3 mM NaH_2PO_4, and 0.1% Tween-20, pH 7.2) before use and detected with Alexa Fluor 680– or 800–conjugated secondary antibodies (1:20,000) imaged using an Odyssey scanning system (LI-COR Biosciences). Primary antibodies used include: anti-GFP (Takara Bio, Inc.), anti-GST (Sigma-Aldrich), anti-Mena2197[43], anti-β3-tubulin (Promega), anti-Robo1 (Abcam), and anti-neurofilament (EMD Millipore).

Plasmids and reagents

Met-Robo cDNA was kindly provided by Elke Stein (Yale University, New Haven, CT) (Stein and Tessier-Lavigne, 2001). RoboCC domains were amplified from Met-Robo cDNA using Phusion polymerase (New England Biolabs, Inc.). Amplified products were inserted into pIC113 (Cheeseman and Desai, 2005; gift from I. Cheeseman, Massachusetts Institute of Technology, Cambridge, MA) between the EcoRI-SalI sites. Mena EVH1 (amino acids 1–115) was amplified by PCR from mouse cDNA and inserted into pGEX2TK (GE Healthcare). Recombinant GST-EVH1 protein was produced in BL-21 *Escherichia coli* and purified using standard methods. Slit2N and Sema3A were purchased from PeproTech.

EVH1 binding assays

For pull-down experiments, GFP-tagged CC domains from rat Robo1 were expressed in HEK293 cells. Cells were washed with PBS, lysed in 1mL ice-cold lysis buffer (10 mM Tris, pH 8.0, 150 mM NaCl, 0.5% Nonidet-P 40, and 1 mM Pefabloc) and centrifuged at 18,000 *g* for 10 min. The supernatant was transferred to a new tube and incubated with 2 µg GST-Mena-EVH1 at 4°C for one hour. A total of 5 µl packed glutathione-agarose resin (Thermo Fisher Scientific) was added and incubated for an additional hour. Resin was pelleted (1,000 *g*, 5 min), the supernatant fraction was collected, and the resin was washed three times with 500 µl lysis buffer. Bound proteins were eluted with boiling Laemmli sample buffer.

Explant culture

All experiments involving the use of mice were performed in accordance with protocols approved by the MIT Committee on Animal Care. DRG were dissected from E12.5 mice, and plated in 35 mm glass bottomed dishes (MatTek Corporation) that had been cleaned with 5 N hydrochloric acid and coated with 0.25 mg/ml poly-D-lysine (Sigma-Aldrich) and 100 µg/ml mouse Laminin 1 (Southern Biotech). DRGs were plated in serum-free Neurobasal medium supplemented with B27, glutamine, and NGF (Gibco), and cultured overnight in a humidified incubator (37°C, 5% CO_2). A single allele of Mena ($m^{+/-}v^{-/-}e^{-/-}$) was sufficient for animal viability and to produce a grossly normal nervous system (Kwiatkowski et al., 2007); DRG from littermate mice possessing one or two alleles of Mena were used as controls for most experiments. For some experiments, DRG from wild-type Swiss-Webster mice containing normal alleles of Mena, VASP, and EVL were used as an additional control. Wild-type and littermate ($m^{+/+}v^{-/-}e^{-/-}$)/($m^{+/-}v^{-/-}e^{-/-}$) DRG explants performed similarly in all assays tested.

Cell culture and transfection

HEK293 cells were grown in DMEM supplemented with 10% FBS; transfection of these cell lines was performed with Lipofectamine2000 according to the manufacturer's protocols (Invitrogen). CAD cells, a subclone of the catecholaminergic Cath.a cell line (Qi et al., 1997), were cultured in a 1:1 mixture of Ham's F12 and Iscove's DMEM supplemented with 10% FBS. For transfection of primary neurons, DRGs from E14.5 embryos were trypsinized for 10 min at 37°, trypsin was inactivated by adding 5 vol DMEM with 10% FBS, triturated, and centrifuged at 100 *g* for 5 min. Then, 100,000 cells were resuspended in 20 µl of Amaxa SCN basic neuron buffer to which 1 µg of plasmid DNA had been added. Nucleofection was performed with an Amaxa Nucleofector II device, using program SCN 5.

Immunofluorescence and imaging

Whole-mount neurofilament staining. Embryos were collected at E10.5 or E12.5 and processed according to Hua et al. (2013). In brief, embryos were bleached (60% MeOH, 20% DMSO, and 20% H_2O_2) at 4°C for 24 h, washed five times in MeOH, and postfixed (80% MeOH and 20% DMSO) at 4°C overnight. Embryos were rehydrated using a MeOH series in PBS dilutions. After rehydration, embryos were incubated in blocking solution (PBS, 0.5% Triton X-100, 20% DMSO, and 5% normal donkey serum) at 4°C overnight. The following day, anti-NF and anti-GAP43 antibodies were added at 1:200 and incubated for 5 d at RT with end-over-end rotation. Embryos were washed at least six times for 1 h in PBST (PBS plus 0.5% Triton X-100) and then incubated with Alexa Fluor–conjugated secondary antibodies (Jackson ImmunoResearch Laboratories, Inc.) diluted 1:500 in blocking buffer for 1 d. After staining, embryos were washed five times in PBST, dehydrated in EtOH, and either stored at −20°C or imaged after clearing in BABB (33% benzyl alcohol and 67% benzyl benzoate). Optical sections were acquired using a laser scanning confocal (Fluoview 1200; 30×/1.05 NA UPlanS Apo, Si immersion objective; Olympus).

Live-cell imaging. E12.5 DRG explants were cultured for 12–18 h after plating; explant media was changed to phenol-red–free Leibovitz's L15 media (Gibco) supplemented with 0.35% BSA before imaging. Differential interference contrast (DIC) videos were acquired on a Nikon Ti microscope equipped with a 37°C environmental chamber, motorized x/y stage, and a Perfect-Focus system to prevent sample drift. Images were acquired using a water immersion objective (40×/1.15 NA Apo LWD; Nikon), and a Coolsnap HQ camera (Roper Scientific) controlled by Nikon Elements software. For analysis of growth cone motility and filopodium lifetime, images were acquired every 15 s; for detailed analysis of filopodium protrusion, images were collected every 5 s. Image stacks were corrected for lateral drift in the image plane using the Template Matching plugin for ImageJ (National Institutes of Health, v1.47m; Q. Tseng, Université Joseph Fourier, Grenoble, France). Only growth cones that were not in contact with other cells and had extended more than 0.3 mm away from the explant were chosen for imaging. Quantification of growth cone area (Fig. 3) was performed by manually outlining the growth cone using a Wacom tablet and measured using ImageJ. Growth cone extension or retraction (Fig. 3) was characterized by generating a kymograph along the direction of growth cone movement using the multiple kymograph plugin for ImageJ (J. Rietdorf and A. Seitz, European Molecular Biology Laboratory, Heidelberg, Germany); the x/y coordinates of the leading edge over time were manually traced in ImageJ and exported to MATLAB (R2013b; MathWorks). Data were normalized so that the

Published April 18, 2016

origin corresponded to the time and position of the leading edge upon stimulation. Mean position and confidence intervals were calculated from these datasets using custom scripts written in MATLAB. Statistical analysis was performed using Prism (v6.0f; GraphPad Software).

Growth cone turning assay. Turning assays were performed according to Pujic et al. (2008). Mock gradients were generated by loading a micropipette (Femtotips; Eppendorf) with imaging media (L15; Gibco) in which a fluorescent dextran marker was dissolved (70 kD Texas red; Life Technologies); Slit gradients used the same media with the addition of 5 nM Slit-2 (Slit2N; PeproTech); HGF gradients used the same media with the addition of 200 ng/ml HGF (PeproTech). Gradients were generated using a PicospritzerIII (Parker Hannifin) set to deliver 100-kPa pulses of 16-ms duration at a 0.8-Hz repetition rate. Growth cone positions were tracked using the Manual Tracking ImageJ plugin (F.P. Cordelieres, Curie Institute, Paris, France) with the point where the axon inserts into the growth cone used as the point of reference; raw data were exported to MATLAB for analysis.

Online supplemental material

Fig. S1 shows characterization of growth cone turning in response to Slit gradients. Fig. S2 shows evolutionary conservation of Ena/VASP binding sites in Robo receptors. Fig. S3 shows characterization of growth cone collapse and retraction in response to a Slit gradient. Fig. S4 shows axon projections in spinal cord coronal and transverse sections. Video 1 shows a wild-type growth cone undergoing Slit-induced filopodium elongation. Video 2 shows a wild-type growth cone undergoing Sema3A-induced collapse without filopodium elongation. Video 3 shows correlative live-cell DIC and immunofluorescence of a wild-type growth cone undergoing Slit-induced filopodium elongation. Video 4 shows a wild-type neuron undergoing Slit-induced filopodium elongation and neurite retraction. Video 5 shows an Ena/VASP null neuron, which lacks filopodia and does not display Slit-induced filopodium formation or elongation or neurite retraction. Online supplemental material is available at http://www.jcb.org/cgi/content/full/jcb.201509062/DC1.

Acknowledgments

The authors would like to thank Elke Stein and I. Cheeseman for reagents, Eliza Vasile and Jeffrey Wyckoff for imaging assistance, Rachael Neve and the MIT Viral Gene Transfer Core for HSV production, Jenny Tadros for assistance with mice, and E. Wang and members of the Gertler laboratory for helpful discussion.

This work was supported by National Institutes of Health grants F32-CA165700 (R.E. McConnell), R01-GM068678 (F.B. Gertler), and P30-CA014051 (F.B. Gertler).

The authors declare no competing financial interests.

Author contributions: R.E. McConnell characterized Slit-induced filopodium dynamics and performed growth cone turning assays. R.E. McConnell and M. Vidaki performed biochemical analyses. R.E. McConnell and A.S. Meyer characterized Slit-induced axon retraction. J.E. van Veen performed spine explant and peptide array overlay experiments. R.E. McConnell performed whole-mount embryo imaging analyses. A.V. Kwiatkowski made the initial observation of midline defects in Ena–VASP null embryos. J.E. van Veen made the initial observation of Slit-induced filopodium elongation. R.E. McConnell and F.B. Gertler wrote the manuscript. All authors read and commented on the manuscript.

Submitted: 14 September 2015
Accepted: 4 March 2016

References

Akin, O., and R.D. Mullins. 2008. Capping protein increases the rate of actin-based motility by promoting filament nucleation by the Arp2/3 complex. *Cell.* 133:841–851. http://dx.doi.org/10.1016/j.cell.2008.04.011

Bashaw, G.J., T. Kidd, D. Murray, T. Pawson, and C.S. Goodman. 2000. Repulsive axon guidance: Abelson and Enabled play opposing roles downstream of the roundabout receptor. *Cell.* 101:703–715. http://dx.doi.org/10.1016/S0092-8674(00)80883-1

Bear, J.E., and F.B. Gertler. 2009. Ena/VASP: towards resolving a pointed controversy at the barbed end. *J. Cell Sci.* 122:1947–1953. http://dx.doi.org/10.1242/jcs.038125

Bear, J.E., J.J. Loureiro, I. Libova, R. Fässler, J. Wehland, and F.B. Gertler. 2000. Negative regulation of fibroblast motility by Ena/VASP proteins. *Cell.* 101:717–728. http://dx.doi.org/10.1016/S0092-8674(00)80884-3

Bear, J.E., T.M. Svitkina, M. Krause, D.A. Schafer, J.J. Loureiro, G.A. Strasser, I.V. Maly, O.Y. Chaga, J.A. Cooper, G.G. Borisy, and F.B. Gertler. 2002. Antagonism between Ena/VASP proteins and actin filament capping regulates fibroblast motility. *Cell.* 109:509–521. http://dx.doi.org/10.1016/S0092-8674(02)00731-6

Bentley, D., and A. Toroian-Raymond. 1986. Disoriented pathfinding by pioneer neurone growth cones deprived of filopodia by cytochalasin treatment. *Nature.* 323:712–715. http://dx.doi.org/10.1038/323712a0

Bray, D., and K. Chapman. 1985. Analysis of microspike movements on the neuronal growth cone. *J. Neurosci.* 5:3204–3213.

Bray, D., P. Wood, and R.P. Bunge. 1980. Selective fasciculation of nerve fibres in culture. *Exp. Cell Res.* 130:241–250. http://dx.doi.org/10.1016/0014-4827(80)90060-9

Brose, K., K.S. Bland, K.H. Wang, D. Arnott, W. Henzel, C.S. Goodman, M. Tessier-Lavigne, and T. Kidd. 1999. Slit proteins bind Robo receptors and have an evolutionarily conserved role in repulsive axon guidance. *Cell.* 96:795–806. http://dx.doi.org/10.1016/S0092-8674(00)80590-5

Byun, J., B.T. Kim, Y.T. Kim, Z. Jiao, E.-M. Hur, and F.-Q. Zhou. 2012. Slit2 inactivates GSK3β to signal neurite outgrowth inhibition. *PLoS One.* 7:e51895. http://dx.doi.org/10.1371/journal.pone.0051895

Carlier, M.F., and D. Pantaloni. 1997. Control of actin dynamics in cell motility. *J. Mol. Biol.* 269:459–467. http://dx.doi.org/10.1006/jmbi.1997.1062

Chédotal, A. 2007. Slits and their receptors. *Adv. Exp. Med. Biol.* 621:65–80. http://dx.doi.org/10.1007/978-0-387-76715-4_5

Cheeseman, I.M., and A. Desai. 2005. A combined approach for the localization and tandem affinity purification of protein complexes from metazoans. *Sci. STKE.* 2005:pl1.

Chen, Z., B.B. Gore, H. Long, L. Ma, and M. Tessier-Lavigne. 2008. Alternative splicing of the Robo3 axon guidance receptor governs the midline switch from attraction to repulsion. *Neuron.* 58:325–332. http://dx.doi.org/10.1016/j.neuron.2008.02.016

Chien, C.-B., D.E. Rosenthal, W.A. Harris, and C.E. Holt. 1993. Navigational errors made by growth cones without filopodia in the embryonic Xenopus brain. *Neuron.* 11:237–251. http://dx.doi.org/10.1016/0896-6273(93)90181-P

Colak, D., S.-J. Ji, B.T. Porse, and S.R. Jaffrey. 2013. Regulation of axon guidance by compartmentalized nonsense-mediated mRNA decay. *Cell.* 153:1252–1265. http://dx.doi.org/10.1016/j.cell.2013.04.056

Cox, E.C., B. Müller, and F. Bonhoeffer. 1990. Axonal guidance in the chick visual system: posterior tectal membranes induce collapse of growth cones from the temporal retina. *Neuron.* 4:31–37. http://dx.doi.org/10.1016/0896-6273(90)90441-H

Dent, E.W., A.V. Kwiatkowski, L.M. Mebane, U. Philippar, M. Barzik, D.A. Rubinson, S. Gupton, J.E. Van Veen, C. Furman, J. Zhang, et al. 2007. Filopodia are required for cortical neurite initiation. *Nat. Cell Biol.* 9:1347–1359. http://dx.doi.org/10.1038/ncb1654

Dent, E.W., S.L. Gupton, and F.B. Gertler. 2011. The growth cone cytoskeleton in axon outgrowth and guidance. *Cold Spring Harb. Perspect. Biol.* 3:a001800. http://dx.doi.org/10.1101/cshperspect.a001800

Fan, J., and J.A. Raper. 1995. Localized collapsing cues can steer growth cones without inducing their full collapse. *Neuron.* 14:263–274. http://dx.doi.org/10.1016/0896-6273(95)90284-8

Fan, J., S.G. Mansfield, T. Redmond, P.R. Gordon-Weeks, and J.A. Raper. 1993. The organization of F-actin and microtubules in growth cones exposed to a brain-derived collapsing factor. *J. Cell Biol.* 121:867–878. http://dx.doi.org/10.1083/jcb.121.4.867

Fricke, C., J.S. Lee, S. Geiger-Rudolph, F. Bonhoeffer, and C.B. Chien. 2001. astray, a zebrafish roundabout homolog required for retinal axon guidance. *Science.* 292:507–510. http://dx.doi.org/10.1126/science.1059496

Gallo, G., and P.C. Letourneau. 2004. Regulation of growth cone actin filaments by guidance cues. *J. Neurobiol.* 58:92–102. http://dx.doi.org/10.1002/neu.10282

Gomez, T.M., and P.C. Letourneau. 2014. Actin dynamics in growth cone motility and navigation. *J. Neurochem.* 129:221–234. http://dx.doi.org/10.1111/jnc.12506

Hansen, S.D., and R.D. Mullins. 2010. VASP is a processive actin polymerase that requires monomeric actin for barbed end association. *J. Cell Biol.* 191:571–584. http://dx.doi.org/10.1083/jcb.201003014

Hansen, S.D., and R.D. Mullins. 2015. Lamellipodin promotes actin assembly by clustering Ena/VASP proteins and tethering them to actin filaments. *eLife.* 4. http://dx.doi.org/10.7554/eLife.06585

Hao, J.C., T.W. Yu, K. Fujisawa, J.G. Culotti, K. Gengyo-Ando, S. Mitani, G. Moulder, R. Barstead, M. Tessier-Lavigne, and C.I. Bargmann. 2001. C. elegans slit acts in midline, dorsal-ventral, and anterior-posterior guidance via the SAX-3/Robo receptor. *Neuron.* 32:25–38. http://dx.doi.org/10.1016/S0896-6273(01)00448-2

Hata, K., K. Kaibuchi, S. Inagaki, and T. Yamashita. 2009. Unc5B associates with LARG to mediate the action of repulsive guidance molecule. *J. Cell Biol.* 184:737–750. http://dx.doi.org/10.1083/jcb.200807029

Hu, H., M. Li, J.-P. Labrador, J. McEwen, E.C. Lai, C.S. Goodman, and G.J. Bashaw. 2005. Cross GTPase-activating protein (CrossGAP)/Vilse links the Roundabout receptor to Rac to regulate midline repulsion. *Proc. Natl. Acad. Sci. USA.* 102:4613–4618. http://dx.doi.org/10.1073/pnas.0409325102

Hua, Z.L., P.M. Smallwood, and J. Nathans. 2013. Frizzled3 controls axonal development in distinct populations of cranial and spinal motor neurons. *eLife.* 2:e01482. http://dx.doi.org/10.7554/eLife.01482

Hung, R.-J., U. Yazdani, J. Yoon, H. Wu, T. Yang, N. Gupta, Z. Huang, W.J.H. van Berkel, and J.R. Terman. 2010. Mical links semaphorins to F-actin disassembly. *Nature.* 463:823–827. http://dx.doi.org/10.1038/nature08724

Hung, R.-J., C.W. Pak, and J.R. Terman. 2011. Direct redox regulation of F-actin assembly and disassembly by Mical. *Science.* 334:1710–1713. http://dx.doi.org/10.1126/science.1211956

Kapfhammer, J.P., B.E. Grunewald, and J.A. Raper. 1986. The selective inhibition of growth cone extension by specific neurites in culture. *J. Neurosci.* 6:2527–2534.

Keleman, K., S. Rajagopalan, D. Cleppien, D. Teis, K. Paiha, L.A. Huber, G.M. Technau, and B.J. Dickson. 2002. Comm sorts robo to control axon guidance at the Drosophila midline. *Cell.* 110:415–427. http://dx.doi.org/10.1016/S0092-8674(02)00901-7

Kidd, T., K. Brose, K.J. Mitchell, R.D. Fetter, M. Tessier-Lavigne, C.S. Goodman, and G. Tear. 1998. Roundabout controls axon crossing of the CNS midline and defines a novel subfamily of evolutionarily conserved guidance receptors. *Cell.* 92:205–215. http://dx.doi.org/10.1016/S0092-8674(00)80915-0

Kidd, T., K.S. Bland, and C.S. Goodman. 1999. Slit is the midline repellent for the robo receptor in Drosophila. *Cell.* 96:785–794. http://dx.doi.org/10.1016/S0092-8674(00)80589-9

Kwiatkowski, A.V., D.A. Rubinson, E.W. Dent, J. Edward van Veen, J.D. Leslie, J. Zhang, L.M. Mebane, U. Philippar, E.M. Pinheiro, A.A. Burds, et al. 2007. Ena/VASP Is Required for neuritogenesis in the developing cortex. *Neuron.* 56:441–455. http://dx.doi.org/10.1016/j.neuron.2007.09.008

Lebrand, C., E.W. Dent, G.A. Strasser, L.M. Lanier, M. Krause, T.M. Svitkina, G.G. Borisy, and F.B. Gertler. 2004. Critical role of Ena/VASP proteins for filopodia formation in neurons and in function downstream of netrin-1. *Neuron.* 42:37–49. http://dx.doi.org/10.1016/S0896-6273(04)00108-4

Long, H., C. Sabatier, L. Ma, A. Plump, W. Yuan, D.M. Ornitz, A. Tamada, F. Murakami, C.S. Goodman, and M. Tessier-Lavigne. 2004. Conserved roles for Slit and Robo proteins in midline commissural axon guidance. *Neuron.* 42:213–223. http://dx.doi.org/10.1016/S0896-6273(04)00179-5

Lowery, L.A., and D. Van Vactor. 2009. The trip of the tip: understanding the growth cone machinery. *Nat. Rev. Mol. Cell Biol.* 10:332–343. http://dx.doi.org/10.1038/nrm2679

Lundström, A., M. Gallio, C. Englund, P. Steneberg, J. Hemphälä, P. Aspenström, K. Keleman, L. Falileeva, B.J. Dickson, and C. Samakovlis. 2004. Vilse, a conserved Rac/Cdc42 GAP mediating Robo repulsion in tracheal cells and axons. *Genes Dev.* 18:2161–2171. http://dx.doi.org/10.1101/gad.310204

Luo, Y., D. Raible, and J.A. Raper. 1993. Collapsin: a protein in brain that induces the collapse and paralysis of neuronal growth cones. *Cell.* 75:217–227. http://dx.doi.org/10.1016/0092-8674(93)80064-L

Ma, L., and M. Tessier-Lavigne. 2007. Dual branch-promoting and branch-repelling actions of Slit/Robo signaling on peripheral and central branches of developing sensory axons. *J. Neurosci.* 27:6843–6851. http://dx.doi.org/10.1523/JNEUROSCI.1479-07.2007

Marsick, B.M., K.C. Flynn, M. Santiago-Medina, J.R. Bamburg, and P.C. Letourneau. 2010. Activation of ADF/cofilin mediates attractive growth cone turning toward nerve growth factor and netrin-1. *Dev. Neurobiol.* 70:565–588. http://dx.doi.org/10.1002/dneu.20800

Mattila, P.K., and P. Lappalainen. 2008. Filopodia: molecular architecture and cellular functions. *Nat. Rev. Mol. Cell Biol.* 9:446–454. http://dx.doi.org/10.1038/nrm2406

Mejillano, M.R., S. Kojima, D.A. Applewhite, F.B. Gertler, T.M. Svitkina, and G.G. Borisy. 2004. Lamellipodial versus filopodial mode of the actin nanomachinery: pivotal role of the filament barbed end. *Cell.* 118:363–373. http://dx.doi.org/10.1016/j.cell.2004.07.019

Menon, S., N.P. Boyer, C.C. Winkle, L.M. McClain, C.C. Hanlin, D. Pandey, S. Rothenfußer, A.M. Taylor, and S.L. Gupton. 2015. The E3 Ubiquitin Ligase TRIM9 Is a Filopodia Off Switch Required for Netrin-Dependent Axon Guidance. *Dev. Cell.* 35:698–712. http://dx.doi.org/10.1016/j.devcel.2015.11.022

Nguyen Ba-Charvet, K.T., K. Brose, V. Marillat, T. Kidd, C.S. Goodman, M. Tessier-Lavigne, C. Sotelo, and A. Chédotal. 1999. Slit2-Mediated chemorepulsion and collapse of developing forebrain axons. *Neuron.* 22:463–473. http://dx.doi.org/10.1016/S0896-6273(00)80702-3

Niclou, S.P., L. Jia, and J.A. Raper. 2000. Slit2 is a repellent for retinal ganglion cell axons. *J. Neurosci.* 20:4962–4974.

Niebuhr, K., F. Ebel, R. Frank, M. Reinhard, E. Domann, U.D. Carl, U. Walter, F.B. Gertler, J. Wehland, and T. Chakraborty. 1997. A novel proline-rich motif present in ActA of Listeria monocytogenes and cytoskeletal proteins is the ligand for the EVH1 domain, a protein module present in the Ena/VASP family. *EMBO J.* 16:5433–5444. http://dx.doi.org/10.1093/emboj/16.17.5433

Peterson, F.C., and B.F. Volkman. 2009. Diversity of polyproline recognition by EVH1 domains. *Front. Biosci. (Landmark Ed.).* 14:833–846. http://dx.doi.org/10.2741/3281

Piper, M., R. Anderson, A. Dwivedy, C. Weinl, F. van Horck, K.M. Leung, E. Cogill, and C. Holt. 2006. Signaling mechanisms underlying Slit2-induced collapse of Xenopus retinal growth cones. *Neuron.* 49:215–228. http://dx.doi.org/10.1016/j.neuron.2005.12.008

Pujic, Z., C.E. Giacomantonio, D. Unni, W.J. Rosoff, and G.J. Goodhill. 2008. Analysis of the growth cone turning assay for studying axon guidance. *J. Neurosci. Methods.* 170:220–228. http://dx.doi.org/10.1016/j.jneumeth.2008.01.014

Qi, Y., J.K.T. Wang, M. McMillian, and D.M. Chikaraishi. 1997. Characterization of a CNS cell line, CAD, in which morphological differentiation is initiated by serum deprivation. *J. Neurosci.* 17:1217–1225.

Raper, J.A., and J.P. Kapfhammer. 1990. The enrichment of a neuronal growth cone collapsing activity from embryonic chick brain. *Neuron.* 4:21–29. http://dx.doi.org/10.1016/0896-6273(90)90440-Q

Raper, J.A., M. Bastiani, and C.S. Goodman. 1983. Pathfinding by neuronal growth cones in grasshopper embryos. I. Divergent choices made by the growth cones of sibling neurons. *J. Neurosci.* 3:20–30.

Robles, E., A. Huttenlocher, and T.M. Gomez. 2003. Filopodial calcium transients regulate growth cone motility and guidance through local activation of calpain. *Neuron.* 38:597–609. http://dx.doi.org/10.1016/S0896-6273(03)00260-5

Ros, O., T. Cotrufo, R. Martínez-Mármol, and E. Soriano. 2015. Regulation of patterned dynamics of local exocytosis in growth cones by netrin-1. *J. Neurosci.* 35:5156–5170. http://dx.doi.org/10.1523/JNEUROSCI.0124-14.2015

Shekarabi, M., and T.E. Kennedy. 2002. The netrin-1 receptor DCC promotes filopodia formation and cell spreading by activating Cdc42 and Rac1. *Mol. Cell. Neurosci.* 19:1–17. http://dx.doi.org/10.1006/mcne.2001.1075

Stein, E., and M. Tessier-Lavigne. 2001. Hierarchical organization of guidance receptors: silencing of netrin attraction by slit through a Robo/DCC receptor complex. *Science.* 291:1928–1938. http://dx.doi.org/10.1126/science.1058445

Tang, F., and K. Kalil. 2005. Netrin-1 induces axon branching in developing cortical neurons by frequency-dependent calcium signaling pathways. *J. Neurosci.* 25:6702–6715. http://dx.doi.org/10.1523/JNEUROSCI.0871-05.2005

Terman, J.R., T. Mao, R.J. Pasterkamp, H.-H. Yu, and A.L. Kolodkin. 2002. MICALs, a family of conserved flavoprotein oxidoreductases, function in plexin-mediated axonal repulsion. *Cell.* 109:887–900. http://dx.doi.org/10.1016/S0092-8674(02)00794-8

Tosney, K.W., and L.T. Landmesser. 1985. Growth cone morphology and trajectory in the lumbosacral region of the chick embryo. *J. Neurosci.* 5:2345–2358.

Vitriol, E.A., and J.Q. Zheng. 2012. Growth cone travel in space and time: the cellular ensemble of cytoskeleton, adhesion, and membrane. *Neuron.* 73:1068–1081. http://dx.doi.org/10.1016/j.neuron.2012.03.005

Waxman, S.G., J.D. Kocsis, and P.K. Stys. 1995. The Axon: Structure, Function, and Pathophysiology. Oxford University Press, New York, NY. 692 pp.

Winkelman, J.D., C.G. Bilancia, M. Peifer, and D.R. Kovar. 2014. Ena/VASP Enabled is a highly processive actin polymerase tailored to self-assemble parallel-bundled F-actin networks with Fascin. *Proc. Natl. Acad. Sci. USA*. 111:4121–4126. http://dx.doi.org/10.1073/pnas.1322093111

Wong, K., X.-R. Ren, Y.-Z. Huang, Y. Xie, G. Liu, H. Saito, H. Tang, L. Wen, S.M. Brady-Kalnay, L. Mei, et al. 2001. Signal transduction in neuronal migration: roles of GTPase activating proteins and the small GTPase Cdc42 in the Slit-Robo pathway. *Cell.* 107:209–221. http://dx.doi.org/10.1016/S0092-8674(01)00530-X

Yu, T.W., J.C. Hao, W. Lim, M. Tessier-Lavigne, and C.I. Bargmann. 2002. Shared receptors in axon guidance: SAX-3/Robo signals via UNC-34/Enabled and a Netrin-independent UNC-40/DCC function. *Nat. Neurosci.* 5:1147–1154. http://dx.doi.org/10.1038/nn956

Yue, X., A.I. Son, and R. Zhou. 2013. Growth cone collapse assay. *Methods Mol. Biol.* 1018:221–227. http://dx.doi.org/10.1007/978-1-62703-444-9_21

Zelina, P., H. Blockus, Y. Zagar, A. Péres, F. Friocourt, Z. Wu, N. Rama, C. Fouquet, E. Hohenester, M. Tessier-Lavigne, et al. 2014. Signaling switch of the axon guidance receptor Robo3 during vertebrate evolution. *Neuron.* 84:1258–1272. http://dx.doi.org/10.1016/j.neuron.2014.11.004